THE ASTROPHYSICAL JOURNAL, 474: 397–406, 1997 January 1

THE STRUCTURE AND EMISSION OF ACCRETION DISKS IRRADIATED BY INFALLING ENVELOPES

PAOLA D'ALESSIO,[1] NURIA CALVET,[2,3,4] AND LEE HARTMANN[3]

Received 1995 December 15; accepted 1996 July 22

ABSTRACT

We calculate the emission from steady viscous disks heated by radiation from an opaque infalling protostellar envelope. For typical envelope parameters used to explain the spectral energy distributions of protostellar sources, we find that the envelope heating raises the outer disk temperature dramatically. The resulting temperature distribution in the disk is a complicated function of both radial distance and vertical height above the disk midplane. We show that the visibility flux at $\lambda = 0.87$ mm and the spectral energy distribution from submillimeter to radio wavelengths of the flat-spectrum T Tauri star HL Tau can be explained by emission from an accretion disk irradiated by its infalling envelope, whereas thermal emission from an infalling envelope or radiation from a steady viscous accretion disk cannot explain the observations. Our results suggest that the radiation fields of collapsing protostellar envelopes may strongly affect the structure of pre–main-sequence accretion disks.

Subject headings: accretion, accretion disks — circumstellar matter — radiative transfer — stars: individual (HL Tauri) — stars: pre–main-sequence

1. INTRODUCTION

Accretion disks around young stellar objects appear as a natural consequence of the gravitational collapse of material with nonzero angular momentum (Cassen & Moosman 1981; Terebey, Shu, & Cassen 1984, hereafter TSC). Although the infrared excess emission of T Tauri stars is usually assumed to arise from dusty circumstellar accretion disks left over from protostellar collapse, many pre–main-sequence stars exhibit flatter spectral energy distributions (SEDs), with more emission at far-infrared wavelengths, than simple models for disk emission would predict (e.g., Lynden-Bell & Pringle 1974). In some cases, for example, the so-called flat-spectrum T Tauri stars, the large mid- and far-infrared emission can be attributed directly to thermal emission from an infalling dusty protostellar envelope (Calvet et al. 1994, hereafter CHKW). However, recent millimeter- and submillimeter-wavelength observations with high spatial resolution (Keene & Masson 1990; Lay et al. 1994, hereafter LCHP; Dutrey et al. 1996), which directly probe disk emission on small radial scales (Terebey, Chandler, & André 1993), indicate that the outer disk temperatures of some objects—including HL Tau—really are much higher than predicted by standard steady disk theory.

Outer disk temperatures can be raised by increasing the heating from external light sources. Kenyon & Hartmann (1987) suggested that the natural curvature or "flaring" of disks might result in more irradiation because this geometry causes the disk to intercept more light directly from the central star. Natta (1993) showed that a dusty envelope of moderate to small optical depth could scatter significant amounts of radiation from the central star into the disk and increase outer disk temperatures substantially. Although this idea is attractive, the origin of the optically thin dusty envelope is not clear. Disk heating by irradiation from optically thick infalling protostellar envelopes was considered by Butner et al. (1991) and Butner, Natta, & Evans (1994), whose spherically symmetric calculations indicated that disk irradiation could be very important in the protostellar phase.

The goal of this paper is to present a preliminary exploration of the effects of radiation from infalling optically thick protostellar envelopes on a standard viscous accretion disk. The essential differences between this work and previous efforts are as follows: first, we use nonspherical symmetric envelope models that extend inward to the dust destruction radius (e.g., $\sim$0.1 AU for the luminosity of HL Tau), and in which we have solved the transfer of radiation at each frequency, including both scattering and emission by the dust particles; second, we consider the effects of the irradiation on the physical state of the accretion disk, treating carefully the interaction of the envelope radiation with the disk and allowing it to have both radial and vertical (i.e., perpendicular to the midplane) temperature gradients. We are motivated to attack this problem in part because two of the brightest objects at submillimeter and millimeter wavelengths in Taurus, L1551 IRS 5 and HL Tau, are thought to be surrounded by dense infalling envelopes (Adams, Lada, & Shu 1987; Butner et al. 1991, 1994; Kenyon, Calvet, & Hartmann 1993a; Kenyon et al. 1993b; Hayashi, Ohashi, & Miyama 1993; CHKW), suggesting a correlation between envelope irradiation and millimeter-wave disk emission.

We show that irradiation by opaque envelopes can strongly elevate outer disk temperatures and may have other interesting physical implications for disks. This contribution represents an initial effort in a program to make detailed predictions which can be tested by current and future millimeter and submillimeter interferometric observations of pre–main-sequence disks. We demonstrate the potential of the observations to constrain disk properties and disk physics by illustrating how our model can explain detailed properties of HL Tau.

[1] Instituto de Astronomía, Universidad Nacional Autónoma de México, Apdo. Postal 70-264, 04510 México D.F., Mexico; dalessio@astroscu.unam.mx.

[2] Five College Astronomy Department, University of Massachusetts, Amherst, MA 10003; ncalvet@medea.harvard.edu.

[3] Harvard-Smithsonian Center for Astrophysics, 60 Garden Street, Cambridge, MA 02138; hartmann@cfassp44.harvard.edu.

[4] On leave from Centro de Investigaciones de Astronomía, Mérida, Venezuela.

2. MODELS

We have calculated time-independent, geometrically thin, viscous accretion disk models using the standard α-viscosity prescription (Shakura & Sunyaev 1973) for which the viscosity coefficient is expressed as $\nu = \alpha c_s H_p$, where c_s is the local sound speed, H_p is the local pressure scale height of the gas, and α is the viscosity parameter (assumed to be constant through the disk). We calculate structures of disks both with and without surrounding envelopes. The rotating and infalling envelope is modeled using the TSC prescription, which has been used to explain the SEDs of protostellar sources with some success (Adams et al. 1987; Kenyon et al. 1993a). For a fixed central mass, the parameters of the TSC envelope model are the infall rate $\dot{M}_{\rm infall}$ and the centrifugal radius R_c, which denotes the largest disk cylindrical radius instantaneously receiving infalling material. We consider both pure TSC models and a modified sheet-collapse version, the latter with reduced envelope extinction along polar directions as required to account for observed scattered-light nebulae (Hartmann, Calvet, & Boss 1996, hereafter HCB). These models require the additional parameter η, which is the cloud radius from which the material infalling at time t originates, in units of a scale height of the original sheet. This parameter is a measure of the flattening of the infalling envelope at a given time (see HCB).

The envelope calculations from CHKW and HCB assume that the luminosity comes from a star and a disk; in the case of HL Tau considered here, $\sim$95% of the luminosity is assumed to be in the disk.

Cassen & Moosman (1981) and Cantó & Moreno (1997) found that, in the case of a disk receiving matter from an infalling envelope, the total flux of energy produced at each radius and the surface density are comparable to those of a steady disk with a uniform $\dot{M}$. However, the mass accretion rate in this case should be equal to the mass infall rate. We find that the family of models that fit our observational constraints can accommodate this condition. Therefore, we will ignore any departure from the steady disk equations in this preliminary investigation, and we will initially focus on the thermal effects of the infalling envelope.

Because we wish to include both internal viscous heating and external irradiation heating, we calculate the vertical structure of the disk using the methods discussed in detail in D'Alessio (1996) and D'Alessio et al. (1997) and briefly summarized here. We assume that the disk is in vertical hydrostatic equilibrium and that it is heated by viscous dissipation at every height, by radiation from the infalling envelope when it is present, by ionization from cosmic rays, which are exponentially attenuated in the vertical direction, and by radioactive decay. The energy is transported in the vertical direction by radiation, convection, and turbulent fluxes, the latter computed self-consistently with the viscosity, assuming that the turbulent elements responsible for the viscous dissipation are transporting energy (see D'Alessio 1996 for details). Radial energy transport is neglected since the disk is assumed to be geometrically thin. Vertical radiative transport is described by the first and second moments of the transfer equation, using the Eddington approximation to close the system:

$$\frac{dF_{\rm rad}}{dz} = 4\pi\kappa_{\rm P}(P, T)\rho\left(\frac{\sigma T^4}{\pi} - J\right), \tag{1}$$

$$\frac{dJ}{dz} = -3\chi_{\rm R}(P, T)\rho\,\frac{F_{\rm rad}}{4\pi} \tag{2}$$

(Mihalas 1978), where $F_{\rm rad}$ is the net flux transported by radiation, J is the mean intensity of the radiation field and both quantities are integrated over frequencies, ρ is the mass density, and $\kappa_{\rm P}(P, T)$ and $\chi_{\rm R}(P, T)$ are Planck and Rosseland mean opacities per unit mass, computed with monochromatic opacities described by Calvet et al. (1991) and D'Alessio (1996). (We note that the use of a Planck mean opacity evaluated at the disk temperature in eq. [1] at all heights in the disk assumes that the envelope radiation field has a characteristic temperature similar to that of the disk; for the parameters adopted here, this appears to be a reasonable first approximation.)

The disk intercepts the radiative flux $F_{\rm irrad}(R)$ from the envelope, but the net surface flux of the disk is equal to the viscous flux. The frequency-integrated mean intensity then can be specified using the two-stream approximation; at the disk surface z_∞, the boundary conditions for equations (1) and (2) can be expressed as

$$F_{\rm rad}(z_\infty) = D(R)\,, \tag{3}$$

$$J(z_\infty) = \frac{\sqrt{3}}{4\pi}\,[D(R) + 2F_{\rm irrad}(R)]\,, \tag{4}$$

where $D(R)$ is the viscous energy flux. The height z_∞ is found as an eigenvalue, using the symmetry requirement that the midplane flux be zero.

The surface brightness distribution of the disk is calculated by solving the transfer equation along rays toward the observer. The millimeter-wave dust opacity, which is an important source of uncertainty in calculating the disk spectral energy distribution and physical properties, is assumed to be a power law for wavelengths greater than 200 μm,

$$\kappa_\nu = \kappa_0\left(\frac{\lambda}{200\ \mu{\rm m}}\right)^{-\beta} \tag{5}$$

(Beckwith et al. 1990), where we have taken β as a free parameter to fit the long-wavelength spectral distribution of a given object. For HL Tau we used $\beta = 1$. The coefficient $\kappa_0 = 0.1$ cm^2 g^{-1} is obtained by assuming that at wavelengths shorter than 200 μm the dust opacity is given by Draine & Lee (1984). Other opacity sources are included in the calculation of the structure and the spectrum of the disk (see Calvet et al. 1991 and D'Alessio 1996 for details): free-free from H^0, H^-, He^-, H_2^-, bound-free from H^0, H^-, Si, Mg, C, He^-, bands from CO, TiO, OH, H_2O, and scattering by H_2, H^0, He^0, and electrons.

The energy per unit area deposited by the envelope at each disk radius R and frequency ν is the component of the vector flux along the disk normal, which is given by

$$F_z(\nu) = \iint I_\nu(\mu, \phi)\mu\, d\mu\, d\phi\,, \tag{6}$$

where $\mu = \cos\theta$ and θ is the inclination to the normal to the disk, which is assumed flat in this calculation; ϕ is the azimuthal angle at the local system of coordinates at R, with axis z coinciding with the normal. The specific intensity $I_\nu(\mu, \phi)$ is calculated by integrating the transfer equation along rays that scan the space above radius R. Along each ray, specified by coordinates (θ, ϕ), the optical depth is calculated by using the angle-dependent density distribution. The emissivity includes both a thermal and a scattering component, assumed to be isotropic; we use the temperature and the mean intensity at each point obtained in the solution of the radiative transfer equations in the spherical equivalent case, with the density equal to the average over angle of the true density (Kenyon et al. 1993a; CHKW). With this procedure, we include the radiation that is scattered toward R from the star and from any other region of the envelope, as well as its thermal emission. We also include the flux coming directly from the star, although usually for the envelopes of the objects included here, it is negligible. The flux deposited in the disk surface, $F_{\rm irrad}(R)$, is the integral over frequency of $F_z(\nu)$.

3. RESULTS

3.1. *Basic Structure of Nonirradiated Disks*

Figure 1 shows temperature distributions of a viscous disk in which effects of irradiation by both the central star and any infalling envelope are omitted. The disk has a mass accretion rate $\dot{M} = 10^{-6}\ M_\odot\ \rm yr^{-1}$, a viscosity parameter $\alpha = 4 \times 10^{-2}$, and a typical T Tauri central star with $R_* = 3\ R_\odot$ and $M_* = 0.5\ M_\odot$.

At a given radius, the difference between the temperature at the disk midplane (T_c) and the temperature at the height where the Rosseland mean optical depth is $\frac{2}{3}$ ($T_{\rm eff}$) reflects the temperature gradient in the vertical direction required to transport the energy released by viscous dissipation at every height. The brightness temperature T_b at $\lambda = 0.87$ mm is also shown, calculated assuming that the disk inclination to the line of sight $\theta = 0$ (i.e., the disk is viewed pole-on). The brightness temperature T_b is defined as $I_\nu = 2k\nu^2 T_b/c^2$, where I_ν is the specific intensity at frequency ν, k is the Boltzmann constant, and c is the speed of light.

Even though the effective temperature distribution of the disk models is essentially a power law and would result in a power-law SED in the infrared spectral regions where the disk is highly opaque (e.g., Lynden-Bell & Pringle 1974), the submillimeter brightness temperature departs very strongly from power-law behavior. In the innermost regions, where the temperature is higher than the typical temperature for dust sublimation, the $\lambda = 0.87$ mm emission is formed at a Rosseland mean optical depth less than $\frac{2}{3}$, and so the brightness temperature falls below the effective temperature. At intermediate radii (0.1 AU $\lesssim R \lesssim$ 30 AU), the submillimeter optical depth of the disk is relatively small, and the emission arises from more central, hotter disk layers, resulting in a brightness temperature that far exceeds the local effective temperature. Finally, at large radii ($R \gtrsim$ 30 AU), the disk is only marginally optically thick and close to isothermal vertically, so the brightness temperature falls below the effective temperature by a factor $\sim\{1 - \exp[-\tau(0.87\ \mu\rm m)]\}$.

3.2. *Structure of Irradiated Disks*

Figure 2 shows the effects on the disk temperature distribution of irradiation from an infalling envelope with $\dot{M}_{\rm infall} = 4 \times 10^{-6}\ M_\odot\ \rm yr^{-1}$ and $R_c = 50$ AU, parameters typically inferred for protostellar sources in the Taurus molecular cloud complex (Kenyon et al. 1993a). The outer disk temperature rises dramatically over that which would

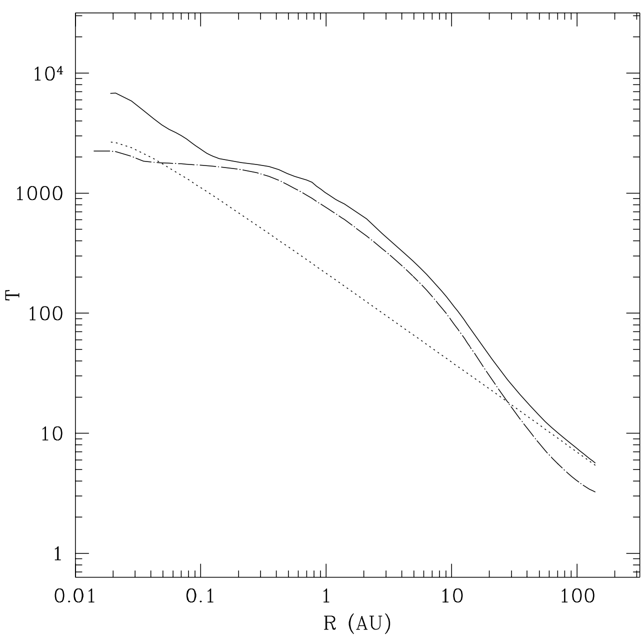

FIG. 1.—Characteristic temperatures for the nonirradiated accretion disk model plotted as a function of radius. The disk has $\dot{M} = 10^{-6}\ M_\odot$ $\rm yr^{-1}$, $\alpha = 0.04$, and the central star has $M_* = 0.5\ M_\odot$ and $R_* = 3\ R_\odot$. The solid line is the midplane temperature T_c, the dotted line shows the effective temperature of a viscous nonirradiated disk $T_{\rm vis}$, and the dot-dashed line is the brightness temperature T_b at $\lambda = 0.87$ mm. In this case, $T_{\rm vis}$ is equal to the temperature $T_{\rm eff}$ calculated as the temperature at the height where $\tau_{\rm R} = \frac{2}{3}$.

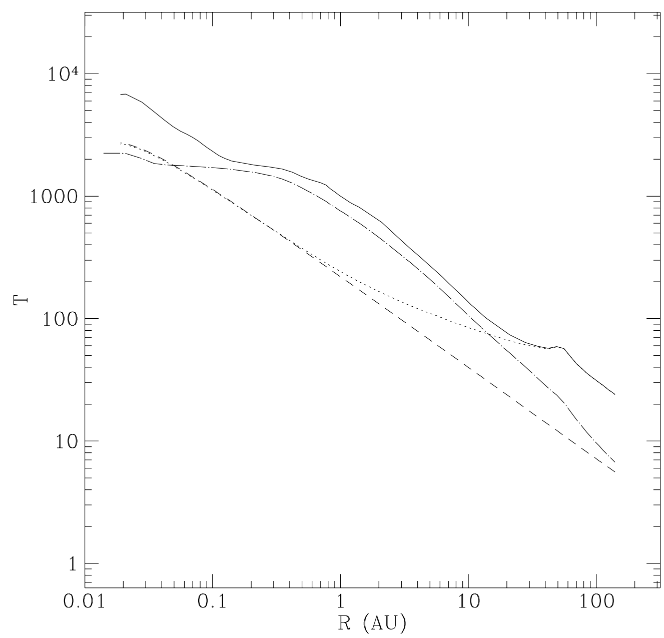

FIG. 2.—Characteristic temperatures for the irradiated accretion disk model plotted as a function of radius. The disk and central star parameters are the same as in Fig. 1. The infalling envelope included as a heating source has $\dot{M}_{\rm infall} = 4 \times 10^{-6}\ M_\odot\ \rm yr^{-1}$, $\eta = 2$, and $R_c = 50$ AU, taken from HCB. (Unless explicitly stated otherwise, this is the envelope model for all the irradiated disk models shown in the following figures). The solid line is the midplane temperature T_c, the dashed line is the effective temperature of a viscous nonirradiated disk $T_{\rm vis}$, the dotted line corresponds to the effective temperature $T_{\rm eff}$ calculated as the temperature at the height where $\tau_{\rm R} = \frac{2}{3}$, and the dot-dashed line is the brightness temperature T_b at $\lambda = 0.87$ mm.

result from pure viscous heating at $R \gg R_*$,

$$T_{\rm eff} = T_{\rm vis} \approx (12\ {\rm K})\left(\frac{R}{50\ {\rm AU}}\right)^{-3/4} \times \left(\frac{M_*}{0.5\ M_\odot}\right)^{1/4}\left(\frac{\dot{M}}{10^{-6}\ M_\odot\ {\rm yr}^{-1}}\right)^{1/4} . \quad (7)$$

At large radii, the irradiating flux is much larger than the local accretion energy release and the envelope radiation penetrates the optically thin regions of the disk, causing the disk to become nearly isothermal vertically, with a temperature given by $\sigma T_{\rm eff}^4 \approx F_{\rm irrad}$; at $R \approx 50$ AU, $T_{\rm eff} \approx T_c \approx 60$ K. It can be shown that the heating by envelope irradiation is much larger than the local accretion energy release as matter falls onto the disk, justifying our neglect of the latter (Cantó & Moreno 1997).

In the context of an α-disk model, the irradiation has an important effect on the disk structure. Figure 3 shows that the surface density drops dramatically at large radii in the irradiated disk relative to the viscous disk. The reason for this can be seen from the steady disk equation for the surface density Σ,

$$\Sigma = \frac{\dot{M}}{3\pi\langle\nu\rangle} \approx \frac{\dot{M}\Omega_{\rm K}}{3\pi\alpha c_s^2(T_c)} = \frac{\dot{M}\Omega_{\rm K}}{3\pi\alpha}\left(\frac{\mu m_{\rm H}}{kT_c}\right) \quad (8)$$

(see, e.g., Frank, King, & Raine 1992, p. 72), where $\langle\nu\rangle$ is a vertically averaged viscosity coefficient, approximated by its value at the disk midplane [i.e., $\langle\nu\rangle \approx \alpha c_s(T_c)H_p(T_c) \approx \alpha c_s^2(T_c)/\Omega_{\rm K}$], H_p is the local scale height of the gas, and $\Omega_{\rm K}$ is the Keplerian angular velocity. We have used here the expression for the sound speed at the disk midplane, $c_s^2(T_c) = kT_c/\mu m_{\rm H}$, where μ is the mean molecular weight, and $m_{\rm H}$ is the mass of a hydrogen atom. The change in disk temperature caused by the irradiation substantially increases the viscosity, and so for a fixed mass accretion rate the surface density drops correspondingly.

This dependence of the surface density on irradiation has an interesting implication for the observed brightness temperature from optically thin regions, given approximately by

$$T_b(R) \approx T_c \frac{\tau_\nu}{\cos\theta} \approx \frac{\kappa_\nu}{\cos\theta}\frac{\dot{M}}{3\pi\alpha}\frac{\Omega_{\rm K}\,\mu m_{\rm H}}{k} , \quad (9)$$

using the solution of the transfer equation in the plane-parallel, optically thin case, and the Rayleigh-Jeans limit for the Planck function. In this equation, the vertical monochromatic optical depth is $\tau_\nu = \kappa_\nu \Sigma$, where κ_ν is given in equation (5), and θ is the inclination angle between the disk normal and the line of sight. Thus the increase of temperature decreases the optical depth in a way that makes T_b independent of the midplane temperature T_c. The practical significance of this result for α-disk models is that, as long as the envelope irradiation heats the disk enough to make its outer parts optically thin, the brightness distribution of these outer annuli is almost independent of the irradiation flux and thus relatively insensitive to the details of the envelope model (Fig. 4).

These results show that, given M_* and R_*, the brightness temperature in the optically thin outer regions of the disk increases proportionally to the ratio $\dot{M}/(\alpha\cos\theta)$ and has a radial dependence approximately given by a power law, $T_b(R) \sim R^{-3/2}$ (Fig. 4). The envelope irradiation increases the brightness of the outer annuli relative to the inner regions of the disk, making the brightness distribution flatter compared with the nonirradiated case. Figure 4 suggests that for a fixed mass infall rate, the results are relatively insensitive to the envelope geometry and to the centrifugal radius R_c. This insensitivity to envelope details means that, to a reasonable approximation, observations at submillimeter and millimeter wavelengths can be fitted by

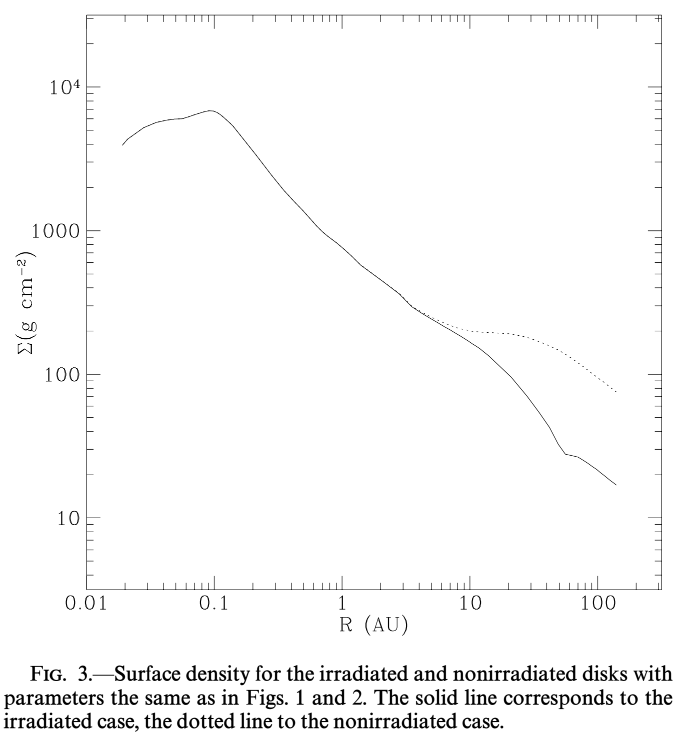

FIG. 3.—Surface density for the irradiated and nonirradiated disks with parameters the same as in Figs. 1 and 2. The solid line corresponds to the irradiated case, the dotted line to the nonirradiated case.

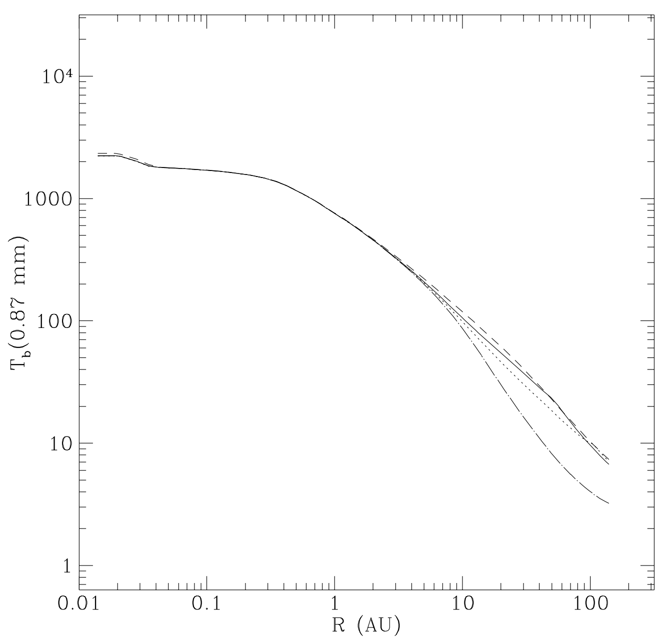

FIG. 4.—Brightness distribution at $\lambda = 0.87\ \mu$m of a disk with parameters the same as in Fig. 1, nonirradiated (*dot-dashed line*) and irradiated by different envelope models: flattened envelopes with $\dot{M}_{\rm infall} = 4 \times 10^{-6}\ M_\odot\ {\rm yr}^{-1}$, $\eta = 2$, $R_c = 50$ AU (*solid line*) and $R_c = 100$ AU (*dotted line*) (taken from HCB), and the initially spherical collapse model from CHKW, with $R_c = 200$ AU and $\dot{M}_{\rm infall} = 4 \times 10^{-6}\ M_\odot\ {\rm yr}^{-1}$ (*dashed line*).

adjusting disk parameters such as the outer disk radius without needing to make corresponding changes in the envelope model.

We have not explored the effects of differing infall rates on the irradiated flux. However, we speculate that our results may not be especially sensitive to modest changes in the infall rate, as long as the envelope remains optically thick. It seems clear that optically thin envelopes of the type discussed by Natta (1993) must intercept a smaller fraction of the central luminosity, and therefore will heat the disk less, than the optically thick envelopes discussed here.

4. APPLICATION TO HL TAURI

HL Tau is a classical T Tauri star with a strong excess emission at both optical-UV and IR wavelengths. The large infrared excess can be explained by radiative equilibrium emission from an infalling dusty envelope (CKHW; HCB). Adopting a mass infall rate typical of Taurus embedded sources, $\sim 4 \times 10^{-6}\ M_\odot\ \mathrm{yr}^{-1}$ (Kenyon et al. 1993a), the infalling envelope model can also explain other observational features such as redshifted C_2 optical absorption lines (Grasdalen et al. 1989), near-infrared scattered-light images (Beckwith et al. 1989), and the velocity pattern seen in spatially resolved ^{13}CO emission (Hayashi et al. 1993). However, this envelope cannot account for the observed continuum flux at wavelengths longer than ~ 1 mm from HL Tau (CKHW; HCB) since the envelope does not contain enough mass at small scales (Terebey et al. 1993).

On the other hand, a circumstellar disk can easily contain enough mass to explain the observed millimeter-wavelength emission of HL Tau if the outer disk temperature is sufficiently high (Beckwith et al. 1990; Beckwith & Sargent 1991). The observations of Lay et al. (1994) indicate that the submillimeter emission of HL Tau is confined to small scales suggestive of a disk. To explain these observations, the disk must have a much flatter temperature distribution than predicted by steady disk theory (Beckwith et al. 1990). In this section we explore whether our envelope-heated disk models can produce the required temperature gradient.

4.1. *Long-Wavelength SED*

Figure 5 shows the observed SED of HL Tau from $\lambda = 10$ μm to 6 cm along with the predictions of different disk models. The observed fluxes (*circles*, *triangles*) were compiled from the literature (Adams, Emerson, & Fuller 1990; Beckwith et al. 1990; Beckwith & Sargent 1991; Brown, Mundt, & Drake 1985; Rodríguez et al. 1992, 1994); the square at $\lambda = 1.3$ cm was calculated by subtracting the flux extrapolated from the SED at longer wavelengths ($\lambda = 3.6$–6 cm), assuming it is emission from the jet, from the flux reported by Rodríguez et al. (1992).

For comparison, we show in Figure 5 the SED of the viscous disk, without irradiation. The absorption feature at ~ 100 μm is due to water vapor formed in the disk *atmosphere* at 0.3 AU $< R <$ 7 AU, with $40 < T < 700$ K. This feature disappears in the irradiated disk because of two reasons: (1) the outer, optically thin disk emission now dominates at $\lambda \sim$ 75–100 μm, since $T \sim 40$ K, and (2) irradiation in the inner optically thick regions ($R \lesssim 10$ AU) increases the temperature and flattens out the temperature profile, decreasing the local absorption strength of the feature.

We also show in Figure 5 the SED of an envelope model with $\dot{M}_{\rm infall} = 4 \times 10^{-6}\ M_\odot\ \mathrm{yr}^{-1}$, $R_c = 50$ AU, and $\eta = 2$.

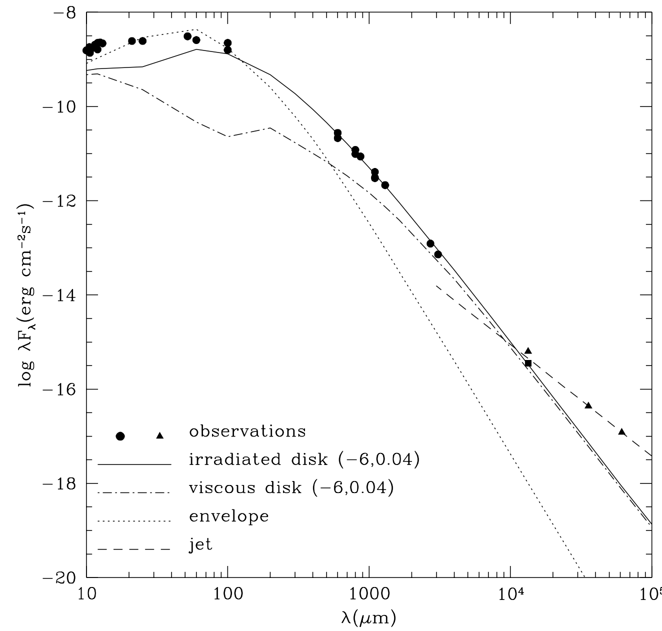

FIG. 5.—Comparison of the spectral energy distribution (SED) of HL Tau with different models. The observations are taken from Adams et al. (1990), Beckwith et al. (1990), and Beckwith & Sargent (1991) (*circles*) and from Brown et al. (1985) and Rodríguez et al. (1992, 1994) (*triangles*). The SED of the disk irradiated by the infalling envelope is plotted with a solid line, and the SED of a nonirradiated disk is plotted with a dot-dashed line. The disk models have $\dot{M} = 10^{-6}\ M_\odot\ \mathrm{yr}^{-1}$, $\alpha = 0.04$, $R_d = 125$ AU, and $\theta = 60°$. Also shown is the SED of an envelope model with $\dot{M}_{\rm infall} = 4 \times 10^{-6}\ M_\odot\ \mathrm{yr}^{-1}$, $R_c = 50$ AU, and $\eta = 2$ (*dotted line*). The dashed line represents the jet emission, given by a power law fitted to the flux at 3.6 and 6 cm. The square at 1.3 cm is calculated by subtracting the flux extrapolated from the SED at longer wavelengths from the flux reported by Rodríguez et al. (1992) (given by the triangle at 1.3 cm).

The outer radius of the infalling region is 2500 AU, and its contribution to the flux beyond ~ 300 μm is negligible compared to that of the disk. The optical depth of the envelope for $\lambda \geq 100$ μm is less than 5×10^{-2}.

We may estimate the accretion rate of the disk models from the accretion luminosity combined with estimates of the mass and radius of the central star. The stellar photospheric emission is strongly veiled in HL Tau by excess hot continuum emission thought to be produced by accretion. The spectral type and luminosity of the central star is uncertain because of the veiling, but it is probably a typical low-mass T Tauri star (Grasdalen et al. 1989). The large veiling continuum suggests that the system luminosity, $L \approx 5\ L_\odot$, is dominated by accretion, so we can neglect the stellar photospheric contribution luminosity of the system to estimate the disk accretion rate (Kenyon et al. 1993a):

$$\dot{M} \approx \frac{R_* L}{G M_*} = (1 \times 10^{-6}\ M_\odot\ \mathrm{yr}^{-1}) \times \left(\frac{L}{5\ L_\odot}\right)\left(\frac{R_*}{3\ R_\odot}\right)\left(\frac{M_*}{0.5\ M_\odot}\right)^{-1} . \quad (10)$$

We assume that the central star is a typical T Tauri object with $M_* \approx 0.5\ M_\odot$ and $R_* \approx 3\ R_\odot$, so that the (inner) disk accretion rate is $\dot{M} \approx 10^{-6}\ M_\odot\ \mathrm{yr}^{-1}$.

In the long-wavelength regime, there are two observable quantities that a model is expected to fit, i.e., the slope of the SED and the flux. As shown in Figure 5, for a nonirradiated accretion disk the slope of the SED from submillimeter to millimeter wavelengths is different from that observed. In this spectral range the SED is dominated by the emission from optically thick regions, and the resulting spectral index, $n = -d \log (\lambda F_\lambda)/d \log \lambda$, tends toward $n \approx 3$, increasing with λ since the contribution from optically thin regions increases.

The irradiation from the envelope makes the outer disk bright and optically thin at submillimeter wavelengths. From equation (9), the emergent flux from the optically thin outer annuli of an α-disk model can be written as

$$F_\nu^{\rm thin} \approx \frac{2}{\lambda^2} \kappa_\nu \frac{\dot{M}}{6\pi\alpha} (GM_*)^{1/2} \mu m_{\rm H} R_d^{1/2} \left[1 - \left(\frac{R_\tau}{R_d}\right)^{1/2}\right], \quad (11)$$

where R_τ is the radius where the disk becomes optically thin. For the irradiated disk, the total emergent flux at submillimeter and millimeter wavelengths is $F_\nu \sim F_\nu^{\rm thin}$, so that the spectral index is given by $n = 3 + \beta$, and the wavelength dependence of the dust opacity determines the slope of the submillimeter-millimeter SED. The flux at a given wavelength is proportional to $\dot{M} R_d^{1/2}/\alpha$ for a fixed central star (R_*, M_*). The inclination angle has no effect on the emergent flux from optically thin regions, but it affects the contribution of the optically thick annuli, which can be $\sim 20\%$ of the total flux at $\lambda \sim 1$ mm.

The submillimeter-millimeter SED ($\lambda \gtrsim 300$ μm) can be used to select a family of irradiated models with an approximately fixed value of $\dot{M} R_d^{1/2}/\alpha$ (see Table 1), given by

$$\left(\frac{\dot{M}}{1 \times 10^{-6}\, M_\odot\ {\rm yr}^{-1}}\right)\left(\frac{\alpha}{4 \times 10^{-2}}\right)^{-1}\left(\frac{R_d}{125\ {\rm AU}}\right)^{1/2} \approx 1\,. \quad (12)$$

For a disk with $\dot{M} = 10^{-6}$ $M_\odot$ yr^{-1}, α cannot be much lower than 0.04 because, as α decreases, the disk optical depth increases and eventually changes the slope of the SED, since the optically thin emission would decrease relative to the optically thick inner disk contribution. In these calculations we have used $\kappa_0 = 0.1$ cm^2 g^{-1} in equation (5); adopting a lower κ_0 implies a lower value of α to fit the SED, given by $\alpha \approx 4 \times 10^{-2}(\kappa_0/0.1)$. Taking $\alpha \approx 0.04$, equation (12) yields a disk radius around $R_d \approx 125$ AU. For a fixed opacity, increasing α decreases the disk optical depth, and a larger disk radius is needed to fit the submillimeter-millimeter fluxes.

Although the irradiated disk has a larger flux compared with the nonirradiated case, it cannot explain the infrared emission at wavelengths smaller than 100 μm. However, in Figure 5 we show that the thermally emitting dusty envelope which produces the irradiation produces enough flux to explain the infrared SED (CHKW; HCB)

TABLE 1

PARAMETERS OF IRRADIATED ACCRETION DISK MODELS FOR HL TAURI[a]

N	$\dot{M}$ ($M_\odot$ yr^{-1})	α	M_d ($M_\odot$)	R_d (AU)	$Q_{\rm T}(R_d)$	R_Q (AU)
1......	2.5×10^{-7}	1×10^{-2}	0.167	125	0.74	98
2......	5×10^{-7}	2×10^{-2}	0.163	125	0.77	100
3......	1×10^{-6}	4×10^{-2}	0.160	125	0.79	100
4......	2.5×10^{-6}	1×10^{-1}	0.156	125	0.80	100
5......	5×10^{-6}	2×10^{-1}	0.152	125	0.80	100
6......	2.5×10^{-7}	8×10^{-3}	0.195	120	0.63	84
7......	1×10^{-6}	5×10^{-2}	0.146	140	0.87	120
8......	1×10^{-6}	3×10^{-2}	0.182	112	0.68	80

[a] Fitting the spectral energy distribution from $\lambda = 1$ mm to $\lambda = 1.3$ cm.

4.2. *Visibility Fluxes of HL Tau*

Circumstellar disks around L1551 IRS 5 and HL Tau have been resolved by LCHP, with the JCMT-CSO two-telescope interferometer at $\lambda = 0.87$ mm. Because it is not possible to make images with a single baseline, results are shown using the visibility flux as a function of both hour angle and the projected length of the baseline, $q = (u^2 + v^2)^{1/2}$, where u and v are the east and north components of the baseline projected on the sky. In the LCHP observations, q varied from 50 to 200 kλ, and the hour angle varied from -5 to $+5$ hr. Here we compare disk model visibility fluxes with the observations of HL Tau.

The visibility flux is the two-dimensional Fourier transform of a source's surface brightness distribution, which has a maximum contribution arising from regions $R_0 \lesssim R \lesssim R_1$, with $R_0 \approx 53[q/(200\ {\rm k}\lambda)]^{-1}[d/(140\ {\rm pc})]$ AU and $R_1 \approx 123[q/(200\ {\rm k}\lambda)]^{-1}[d/(140\ {\rm pc})]$ AU, corresponding to the first and second roots of the zeroth-order Bessel function, taking d as the distance in parsecs to the source (e.g., Arfken 1985). The HL Tau visibility flux in the range observed by LCHP provides information about the brightness distribution of the source between approximately 50 and 200 AU. To interpolate in the two-dimensional Fourier transform along the u-v track of the interferometer, we have to specify the disk inclination angle θ, as well as the position angle γ between the disk major axis and north, for which we have taken $\gamma = 126°$, the value reported by LCHP.

Figure 6 shows the visibility flux observations of HL Tau at 0.87 mm by LCHP. We show both the Gaussian fit (*heavy dashed line*) and the scatter of the observations (*box*). Because the visibility is a positive quantity, the noise distribution is described by a Rice distribution, so that there are more data points above the Gaussian than below (see LCHP)

We also show in Figure 6 the visibility flux of viscous disks without irradiation. The slope of the predicted visibility flux versus projected baseline is much flatter than observed, indicating that the surface brightness distributions (and thus the temperatures) decline too rapidly with increasing radius. The visibility at every q and the slope increase with $\dot{M}$ but are only slightly affected by α, as is expected for an optically thick disk. The total flux changes with the inclination angle as the projected area in the sky, proportional to cos θ, consistent with emission dominated by optically thick regions. We have found no combination of nonirradiated viscous disk parameters to account for the visibility flux of HL Tau.

In Figure 6 we show the visibility flux calculated by *adding* the emission of an infalling envelope model to the emission of the viscous nonirradiated disks. The envelope has $\dot{M}_{\rm infall} = 1.3 \times 10^{-4}$ $M_\odot$ yr^{-1} and the temperature structure given by CHKW. With this $\dot{M}_{\rm infall}$, the envelope model can account for the submillimeter SED of HL Tau.

We find that, despite being overdense (~ 20 times denser than the envelope that fits the IR energy distribution; CHKW; HCB), this envelope contributes to the visibility mostly at projected baselines lower than $q = 50$ kλ (as can be seen in Fig. 6, for the disk with $\dot{M} = 10^{-6}$ $M_\odot$ yr^{-1}) and cannot explain the observed HL Tau visibility flux (see also Terebey et al. 1993). In principle, a very dense envelope could be important in setting the emergent flux over scales larger than ~ 200 AU, but as pointed out by LCHP, the interpolated single-dish flux (Beckwith & Sargent 1991) is

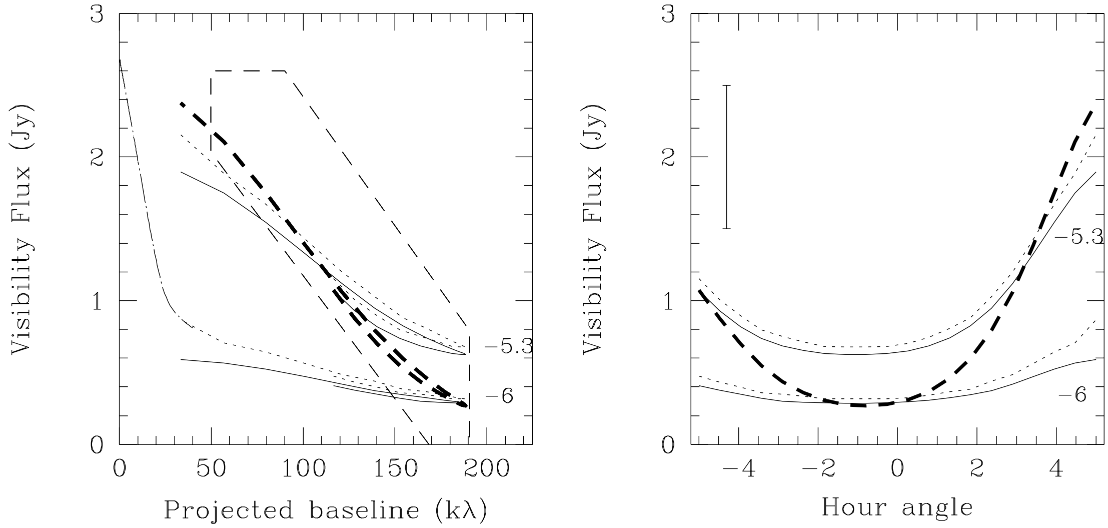

FIG. 6.—Visibility flux at 0.87 mm vs. projected baseline (*left*) and vs. hour angle (*right*) for nonirradiated accretion disk models. The box in the left panel represents the observed HL Tau visibility, and the heavy dashed lines in both panels are the Gaussian fit to the observed visibility (both taken from LCHP). The vertical line in the right panel represents the scatter in the observations. The solid lines correspond to the visibility of the disk models with mass accretion rates $\dot{M} = 10^{-6}$ and $5 \times 10^{-6}\ M_\odot\ \mathrm{yr}^{-1}$. The dotted lines correspond to the visibility of the disks plus a spherically symmetric envelope with $\dot{M}_{\rm infall} = 1.3 \times 10^{-4}\ M_\odot\ \mathrm{yr}^{-1}$, $R_{\rm env} = 1000$ AU, and the temperature structure given by CHKW. The disks have $\alpha = 0.01$, $R_d = 140$ AU, $\theta = 60°$, $\gamma = 126°$, and $\beta = 1$ and the central star has $M_* = 0.5\ M_\odot$ and $R_* = 3\ R_\odot$. In the case of the disk with $\dot{M} = 10^{-6}\ M_\odot\ \mathrm{yr}^{-1}$ in the left panel, we also present the visibility of the disk plus the envelope extended to shorter projected baselines than the minimum detectable by the interferometer (*dash-dotted line, at left*) to show that the contribution of the emission of even this dense envelope model only increases the total flux at 0.87 mm at larger scales (smaller baselines) than those that can be detected with the JCMT-CSO interferometer.

almost equal to the flux obtained with the interferometer, so the envelope's contribution to the total flux at this wavelength must be unimportant.

Figure 7 shows the visibility flux at 0.87 mm versus projected baseline (*left*) and versus hour angle (*right*) for three models of irradiated accretion disks that fit the long-wavelength SED, satisfying equation (12). The models have $R_d = 125$ AU and $\gamma = 126°$, and the other parameters are (1) $\dot{M} = 10^{-6}\ M_\odot\ \mathrm{yr}^{-1}$, $\alpha = 0.04$, and $\theta = 62°$; (2) $\dot{M} = 5 \times 10^{-7}\ M_\odot\ \mathrm{yr}^{-1}$, $\alpha = 0.02$, and $\theta = 60°$; (3) $\dot{M} = 2.5 \times 10^{-7}\ M_\odot\ \mathrm{yr}^{-1}$, $\alpha = 0.01$, and $\theta = 60°$. The irradiated disks yield an excellent fit to the observed slope of the visibility.

We find that for larger outer disk radii, the disk becomes more resolved and more luminous and has a steeper slope to its visibility flux as a function of baseline. The best fits correspond to outer disk radii 110 AU $\lesssim R_d \lesssim$ 140 AU. Changing the inclination angle tends to change the maximum and minimum visibilities together, so that the slope does not change very much. Our best fits have $\theta \sim 60°$, consistent with emission not being resolved along the minor axis by LCHP. The total flux does not change with position angle γ, but the latter parameter does change the visibility flux at the minimum, as well as the hour angle of the minimum. The best fits are for $116° < \gamma < 126°$, in agreement with the results of LCHP. Our results show that

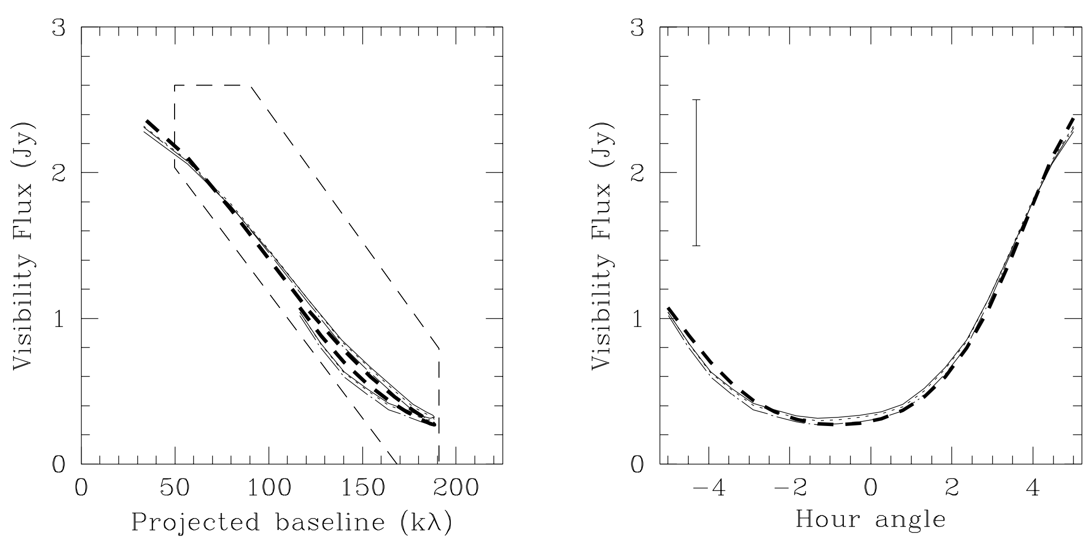

FIG. 7.—Visibility flux at 0.87 mm vs. projected baseline length (*left*) and vs. hour angle (*right*) for irradiated accretion disk models. As in Fig. 6, the box at the left represents the observed HL Tau visibility, and the heavy dashed lines in both panels are the Gaussian fit to the observed visibility. The disk models have log $\dot{M} = -6.6$, $\alpha = 0.01$, and $\theta = 60°$ (*dot-dashed line*), log $\dot{M} = -6.3$, $\alpha = 0.02$, and $\theta = 60°$ (*dotted line*), and log $\dot{M} = -6.0$, $\alpha = 0.04$, and $\theta = 62°$ (*solid line*). The disk radius is $R_d = 125$ AU, and the position angle of the major axis is $\gamma = 126°$.

a steady, viscous disk, irradiated by an infalling envelope consistent with the infrared emission of HL Tau, has a sufficiently flat brightness distribution to reproduce the observed visibility fluxes.

4.3. *Predictions for Other Instruments and Wavelengths*

One of the strengths of the complex disk modeling we have undertaken is that, having fixed parameters to fit one set of data, we can make predictions for other wavelengths and resolutions to test the model.

We multiply the predicted visibility flux of the disk by a "pillbox" function, which is the Fourier transform of the beam, and antitransform the resulting function to obtain the convolved map. In Table 2, we list the semimajor radius of the convolved intensity distribution at half-maximum $R_{1/2}$ of our standard irradiated disk model for HL Tau ($\dot{M} = 1 \times 10^{-6}\ M_\odot\ \mathrm{yr}^{-1}$, $\alpha = 4 \times 10^{-2}$, $\theta = 60°$, $R_d = 125$ AU). The "pillbox" has a radius given by $B_{\max}/\lambda$, and the full width of the beam at half-maximum is $0.705\lambda/B_{\max}$, where $B_{\max}$ is the maximum antenna separation (Thompson, Moran, & Swenson 1986). This value corresponds approximately to the resolution of a uniform-weighted map, θ, listed in Table 2.

All the models that satisfy equation (12) have similar brightness distributions, corresponding to almost the same values of $R_{1/2}$. We find that as long as the disk is large enough to be resolved, its radius at half-maximum brightness is close to the minimum radius detectable by a given instrument. This result is a consequence of the brightness temperature radial distribution of the optically thin annuli, which can be approximated by a power law for $\lambda > 200\ \mu$m (see Fig. 4); the convolution of a power law with the instrumental response produces an image with a size of the order of one-half of the instrumental resolution (see, e.g., Terebey et al. 1993). The last column in Table 2 shows the radius where $\tau_\nu/\cos\theta = 1$. Carlstrom et al. (1995) have suggested the possibility that the measured $R_{1/2}$ reflects the radii where $\tau_\nu/\cos\theta = 1$, but for the model we have presented here, $R_{1/2}$ is strongly dependent upon the instrumental resolution and not on the radius where the disk becomes optically thin.

TABLE 2

HL TAURI DISK RADIUS

Telescope/λ_{obs}	$R_{1/2}$[a] (arcsec)	$\theta/2$[b] (arcsec)	R_{τ_ν}[c] (arcsec)
VLA A:			
3.6 cm	0.1	0.09	0.007
2 cm	0.61	0.05	0.0065
1.3 cm	0.36	0.03	0.015
7 mm	0.025	0.02	0.035
VLA B:			
3.6 cm	0.30	0.25	0.007
2 cm	0.17	0.14	0.0065
1.3 cm	0.13	0.1	0.015
7 mm	0.068	0.05	0.035
VLA C:			
3.6 cm	0.8[d]	0.8	0.007
2 cm	0.49	0.4	0.0065
1.3 cm	0.36	0.3	0.015
7 mm	0.21	0.17	0.035
VLA D:			
3.6 cm	3[d]	3	0.007
2 cm	1.4[d]	1.4	0.0065
1.3 cm	1[d]	1	0.015
7 mm	0.5	0.5	0.035
JCMT-CSO, 0.87 mm	0.45	0.4	0.35
OVRO:			
2.6 mm	1[d]	1	0.15
1.3 mm	0.5	0.5	0.3
BIMA A, 3 mm	1[d]	1	0.125

[a] Apparent disk semimajor axis at half-maximum brightness for model 3 in Table 1.
[b] Half-beamwidth a half-power.
[c] Radius at which $\tau/\cos\theta = 1$.
[d] Not resolved disk.

5. DISCUSSION

Our results show that irradiation of a circumstellar disk by an optically thick infalling envelope can quantitatively explain the high outer disk temperatures required by submillimeter and millimeter observations of HL Tau, the prototypical flat-spectrum T Tauri star. This result appears to be fairly robust because the envelope heating dominates the outer disk temperature distribution, not the assumed viscous accretion processes, and the envelope emission has been determined by modeling completely independent constraints (the SED between $1\ \mu\mathrm{m} \lesssim \lambda \lesssim 100\ \mu$m; CHKW; HCB). The importance of envelope heating that we find is qualitatively consistent with the estimates of Butner et al. (1991, 1994) for spherically symmetric envelopes.

Other aspects of our calculations are uncertain because they are more strongly parameter dependent, or constrained by our assumption of steady α-disk physics, and of course are affected by uncertainties in the adopted dust opacity (e.g., Pollack et al. 1994). Nevertheless, detailed models can be useful in illustrating potential pitfalls of current assumptions used to interpret observations. Our models suggest that disk temperatures may not generally be power laws as a function of radius; moreover, it may not generally be correct to use temperature distributions derived from infrared SEDs to predict submillimeter and millimeter dust emission. For HL Tau, we argue that the infrared and millimeter emission arises from different components (envelope and disk), so that the temperature distribution of one component does not simply translate into the temperature distribution of the other component. Beyond this, our models suggest that even without envelope emission, the effective temperature distribution of the optically thick disk regions emitting in the infrared range may differ from the temperature distribution observed for emission in the submillimeter range (Fig. 1). The importance of this effect for interpreting submillimeter and millimeter fluxes in terms of disk masses will probably depend on how optically thick a given disk is, which could differ from object to object.

Given current disk opacity estimates, various interpretations of the millimeter fluxes from HL Tau suggest that its disk is very massive (Beckwith & Sargent 1991). For a nonirradiated disk with $\dot{M} = 10^{-6}\ M_\odot\ \mathrm{yr}^{-1}$, $\alpha = 4 \times 10^{-2}$, and $R_d \approx 120$ AU, which yields approximately the correct flux at $\lambda \gtrsim 3.6$ cm, the disk mass is $M_d \approx 0.6\ M_\odot$. Our irradiated disk models with the appropriate flux distributions at submillimeter and millimeter wavelengths have estimated disk masses $\sim$0.15–0.2 $M_\odot$ (Table 1). The irradiated disk results agree well with the estimate $M_d = 0.1\ M_\odot$ of Beckwith et al. (1990).

With such large disk masses, the question of gravitational stability arises. The Toomre stability parameter Q_T is given by

$$Q_T = \frac{c_s(T)\Omega_K}{\pi G \Sigma} \approx \frac{3\alpha c_s^3}{G\dot{M}} , \quad (13)$$

where the last approximation is valid for the isothermal optically thin outer annuli. The regions of the disk where $Q_T \geq 1$ are gravitationally stable against axisymmetric perturbations. For a ratio $\dot{M}/\alpha$ given by the brightness of the observed source and an infalling envelope model, which determines the outer disk temperature, the function $Q_T(R)$ is fairly well constrained.

In Table 1, we list the values of Q_T at $R = R_d$ and also the radius R_Q where $Q_T = 1$ for the different models. In Figure 8, Q_T is plotted as a function of R for the same disk, with $\dot{M} = 10^{-6}$ $M_\odot$ yr^{-1} and $\alpha = 4 \times 10^{-2}$, irradiated and nonirradiated. The nonirradiated disk is unstable for $R > R_Q \approx 25$ AU (and is also inconsistent with the long-wavelength flux distribution). In the irradiated case, for a flattened envelope with $R_c = 50$ AU, $R_Q \approx 100$ AU, and $Q_T(R_d = 125$ AU$) \approx 0.7$, then only the outer annuli are gravitationally unstable, with $Q_T \sim 1$.

Viewing this result in a more general way, we may consider our detailed α-disk modeling as no more than a method to arrive at a disk structure, i.e., a disk temperature and density distribution, that is consistent with observational constraints. In this view, we have shown that we can match current observational constraints on the disk of HL Tau with a disk that is marginally unstable to gravitational perturbations in its outermost regions and gravitationally stable at smaller radii, given the current calibration of dust opacity to gas mass. This result might be expected on very general grounds for a disk still rapidly gaining mass from an infalling envelope. The infall preferentially adds mass to the outer edge of the disk, driving it toward instability, but the rapid angular momentum transfer that might result from gravitational instability could increase the accretion rate, reducing the disk mass and helping to prevent Q_T from dropping to very low values (Lin & Pringle 1990).

Our models do not directly constrain mass fluxes through the outer disk, because the viscosity is unknown. Viewing our results from the point of view of empirical modeling, where the (optically thin) disk temperature is determined by the independently determined envelope emission, the surface density is determined from the observed fluxes, which in turn constrains the parameter combination $\dot{M}/\alpha$. For mass accretion rates comparable to the $\dot{M} \approx 10^{-6}$ $M_\odot$ yr^{-1} rate estimated for the inner disk from the accretion luminosity, or for the $\dot{M} \approx 4 \times 10^{-6}$ $M_\odot$ yr^{-1} needed to prevent mass from piling up in the disk due to the infalling envelope, $\alpha \sim 0.04$–0.2. Such large values of α imply viscous timescales for mass transfer

$$t_v \sim \alpha^{-1}(R/H)^2 t_{\rm orbital} \sim 10^5 \text{ yr} \quad (14)$$

(see Pringle 1981). This timescale is sufficiently short that our assumption of steady disk accretion while ignoring the mass addition of infall is not very poor. Similar values of α are required if 100 AU disks with typical values $H/R \sim 0.1$ will evolve on the required disk lifetimes of T Tauri stars (see Edwards et al. 1994). However, these relatively large values for the viscosity parameter are inconsistent with the $\alpha \sim 10^{-3}$ to 10^{-4} required by Bell & Lin (1994) in their *inner* disk models for FU Orionis outbursts. One resolution of this discrepancy may be that the effective value of α is not constant and is much larger at larger disk radii than in the inner disk. This might occur if gravitational instabilities, which are likely to be most important at large disk radii, are important in angular momentum transfer (Lin & Pringle 1990).

Finally, we point out again that an outer disk $\dot{M}$ equal to $\dot{M}_{\rm infall}$ is well within the constraints imposed by our modeling of the SED and 0.87 mm visibility flux. If this is the case, it is then necessary to assume, given the limited accretion luminosity, that material is piling up in the inner disk, perhaps to trigger FU Orionis outbursts (Lin et al. 1994).

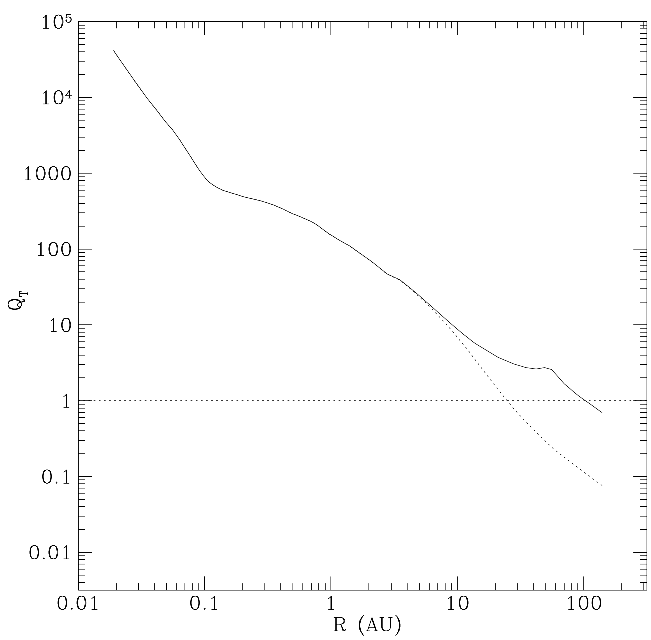

FIG. 8.—Toomre's stability parameter Q_T for a disk with $\dot{M} = 10^{-6}$ $M_\odot$ yr^{-1} and $\alpha = 0.04$ and a central star with $M_* = 0.5$ $M_\odot$ and $R_* = 3$ $R_\odot$. The dotted line represents Q_T for a nonirradiated disk, and the solid line corresponds to an irradiated disk. The horizontal dotted line corresponds to $Q_T = 1$. Regions where $Q_T < 1$ are unstable.

6. SUMMARY

We have shown that the emission of an infalling envelope can be an important heating source of the outer regions in accretion disks around very young stars. We are able to reproduce the SED of the flat-spectrum T Tauri star HL Tau from submillimeter to radio wavelengths, as well as the visibility flux at $\lambda = 0.87$ mm, with an accretion disk irradiated by an infalling envelope. Our disk modeling suggests that the outer disk of HL Tau is near the limit at which gravitational instabilities become important. Our models make the further prediction that the apparent disk radius of HL Tau observed with other instruments at different wavelengths will strongly depend on the spatial resolution of the observations.

Our results generally support the idea that the ultimate energy source of accretion resides at small radii, close to the star. Radiative equilibrium between the central energy sources, the infalling envelope, and the disk can explain the observed brightness temperatures of the outer disk without recourse to unknown heating mechanisms. The visibility fluxes and the long-wavelength SEDs of young stellar objects are powerful constraints on disk properties.

We are grateful to Luis Felipe Rodríguez, Edward Ladd, Andy Harris, Jorge Cantó, Susana Lizano, Steve Strom, Susan Edwards, Javier Ballesteros, Lori Allen, Mike Mayer, and Salvador Curiel for helpful discussions. P. D. would like to thank Steve Strom and the Five College Astronomy Department for their hospitality during her visit. We thank our second referee, Antonella Natta, for her prompt response and comments, which helped us clarify some issues. This work was supported in part by Instituto de Astronomía, UNAM, Mexico, NASA grant NAGW-2306, NSF grant AST-9023554, and STScI grant GO-5355.01.93A.

REFERENCES

Adams, F. C., Emerson, J. P., & Fuller, G. A. 1990, ApJ, 357, 606
Adams, F. C., Lada, C. J., & Shu, F. H. 1987, ApJ, 312, 788
Arfken, G. 1985, Mathematical Methods for Physicists (3d ed.; Orlando: Academic)
Beckwith, S. V. W., Koresko, C. D., Sargent, A. I., & Weintraub, D. A. 1989, ApJ, 343, 393
Beckwith, S. V. W., & Sargent, A. I. 1991, ApJ, 381, 250
Beckwith, S. V. W., Sargent, A. I., Chini, R. S., & Güsten, R. 1990, AJ, 99, 1024
Bell, K. R., & Lin, D. N. C. 1994, ApJ, 427, 987
Brown, A., Mundt, R., & Drake, S. A. 1985, in Radio Stars, ed. R. M. Hjellming & D. M. Gibson (Dordrecht: Reidel), 105
Butner, H. M., Evans, N. J., II, Lester, D. F., Levreault, R. M., & Strom, S. E. 1991, ApJ, 376, 636
Butner, H. M., Natta, A., & Evans, N. J., II. 1994, ApJ, 420, 326
Calvet, N., Hartmann, L., Kenyon, S., & Whitney, B. 1994, ApJ, 434, 330 (CHKW)
Calvet, N., Patiño, A., Magris, G., & D'Alessio, P. 1991, ApJ, 380, 617
Cantó, J., & Moreno, E. 1997, in preparation
Carlstrom, J. E., Lay, O. P., Hill, R. E., & Phillips, T. G. 1995, in Circumstellar Disks, Outflows and Star Formation, ed. S. Lizano & J. M. Torrelles (Rev. Mexicana Astron. Astrofis. Ser. Conf., 1) (México, D.F.: Inst. Astron., Univ. Nac. Autónoma de México), 355
Cassen, P., & Moosman, A. 1981, Icarus, 48, 353
D'Alessio, P. 1996, Ph.D. thesis, Univ. Nac. Autónoma de México
D'Alessio, P., Cantó, J., Lizano, S., & Calvet, N. 1997, in preparation
Draine, B. T., & Lee, H. M. 1984, ApJ, 285, 89
Dutrey, A., Guilloteau, S., Duvert, G., Prato, L., Simon, M., Schuster, K., & Menard, F. 1996, A&A, 309, 493
Edwards, S., Hartigan, P., Ghandour, L., & Andrulis, C. 1994, AJ, 108, 1056
Frank, J., King, A. R., & Raine, D. J. 1992, Accretion Power in Astrophysics (2d ed.; Cambridge: Cambridge University Press)
Grasdalen, G. L., Sloan, G., Stout, M., Strom, S. E., & Welty, A. D. 1989, ApJ, 339, L37
Hartmann, L., Calvet, N., & Boss, A. P. 1996, ApJ, 464, 387 (HCB)
Hayashi, M., Ohashi, N., & Miyama, S. 1993, ApJ, 418, L71
Keene, J., & Masson, C. R. 1990, ApJ, 355, 635
Kenyon, S. J., Calvet, N., & Hartmann, L. 1993a, ApJ, 414, 676
Kenyon, S. J., & Hartmann, L. 1987, ApJ, 323, 714
Kenyon, S. J., Whitney, B. A., Gomez, M., & Hartmann, L. 1993b, ApJ, 414, 773
Lay, O. P., Carlstrom, J. E., Hill, R. E., & Phillips, T. G. 1994, ApJ, 434, L75 (LCHP)
Lin, D. N. C., Hayashi, M., Bell, K. R., & Ohashi, N. 1994, ApJ, 435, 821
Lin, D. N. C., & Pringle, J. E. 1990, ApJ, 358, 515
Lynden-Bell, D., & Pringle, J. E. 1974, MNRAS, 168, 603
Mihalas, D. 1978, Stellar Atmospheres (2d ed.; San Francisco: W. H. Freeman)
Natta, A. 1993, ApJ, 412, 761
Pollack, J. B., Hollenbach, D., Beckwith, S., Simonelli, D. P., Roush, T., & Fong, W. 1994, ApJ, 421, 615
Pringle, J. E. 1981, ARA&A, 19, 137
Rodríguez, L. F., Cantó, J., Torrelles, J. M., Gómez, J. F., Anglada, G., & Ho, P. T. P. 1994, ApJ, 427, L103
Rodríguez, L. F., Cantó, J., Torrelles, J. M., Gómez, J. F., & Ho, P. T. P. 1992, ApJ, 393, L29
Shakura, N. I., & Sunyaev, R. A. 1973, A&A, 24, 337
Terebey, S., Chandler, C. J., & André, P. 1993, ApJ, 414, 759
Terebey, S., Shu, F. H., & Cassen, P. 1984, ApJ, 286, 529 (TSC)
Thompson, A. R., Moran, J. M., & Swenson, G. W. 1986, Interferometry and Synthesis in Radio Astronomy (New York: Wiley)